RSC Sustainability

ROYAL SOCIETY OF CHEMISTRY

PAPER

View Article Online
View Journal

Cite this: DOI: 10.1039/d5su00888c

Double decarbonylation of terephthaloyl chloride: a dual versatile route to *para*-dichlorobenzene in liquid and gas phases

Antoine Beuque, *[a] Marc-Olivier Simon,[b] Emmanuel Marx,[b] Jérémie Zaffran,[c] Pierre de Frémont,[c] Sergio Mastroianni[b] and Stéphane Jeol[b]

Received 27th November 2025
Accepted 27th May 2026

DOI: 10.1039/d5su00888c

rsc.li/rscsus

Recent advances in innovative recycling technologies enable the efficient recovery of high-quality monomers like terephthalic acid (TPA) from polyethylene terephthalate (PET) waste. Building on these advancements, Syensqo aims to produce sustainable high-performance polymers, such as Ryton® polyphenylene sulfide (PPS), using TPA as a starting material. To address this alternative, the double decarbonylation of terephthaloyl chloride (TdCl), derived from TPA, to produce *para*-dichlorobenzene (*p*-DCB), a key monomer of PPS, was evaluated. Two types of processes were assessed: liquid and gas phase decarbonylation. Both approaches achieved a similar turnover frequency of ~30 h^{-1} in *p*-DCB. In the liquid phase, the Wilkinson catalyst $RhCl(PPh_3)_3$ allows the transformation of TdCl into *p*-DCB with a maximum yield of 90% obtained under inert and solvent-free conditions in 4 hours at 220 °C. However, this route was hindered by the formation of regulated by-products, raising environmental concerns. In the gas-phase reaction, Pd-based catalysts were used, achieving up to 95% yield to *p*-DCB in 1 hour at 360 °C, with a total weight hourly space velocity (WHSV) of 25 h^{-1}. Switching the catalyst support from alumina to carbon significantly enhanced the catalytic activity by promoting the formation of an active carbide phase and reducing catalyst deactivation. Finally, a full manufacturing cost (FMC) assessment from TPA to *p*-DCB, covering variable costs, fixed costs, and its environmental footprint, is reported.

Sustainability spotlight

This research is a collaboration between the industrial stakes of Syensqo and the academic expertise of the CNRS. The study explores alternative pathways, derived from terephthalic acid, to produce *para*-dichlorobenzene, a key monomer of polyphenylene sulfide, used in industrial applications. By optimizing experimental conditions, reducing energy consumption, and minimizing chemical waste and impurities, this work directly contributes to the UN Sustainable Development Goals (SDGs). It aligns synergically with SDG 8 (decent work and economic growth) and SDG 9 (industry, innovation, and infrastructure) by fostering sustainable economic growth through open innovation and collaboration for industrial interests. This research advances more innovative and environmentally conscious industrial solutions, contributing to a greener and more sustainable future for the chemical industry.

1. Introduction

The steady accumulation of plastic waste constitutes a significant environmental threat to ecosystems across the globe. Each year, more than 350 million tons of plastic are produced, generating more than 240 million tons of waste. Of this total, only 16% of wastes are recycled, while the rest is incinerated (25%), unmanaged (19%) or accumulated in landfill (40%).[1,2]

Polyethylene terephthalate (PET), widely used in packaging, textiles, and beverage containers, represents approximately 10% of global synthetic plastic production.[3,4] Estimates indicate that PET plastics require several hundred years to fully degrade in the environment through microbial activity, releasing toxic volatile aromatic compounds (benzene, toluene, *etc.*). In this context, recycling technologies have gained prominence to address this substantial fraction of untreated waste.[5–7]

While mechanical recycling remains the most widely used method for PET recovery, it faces major challenges including the necessity for clean and uncontaminated feedstock. Thermal and mechanical molecular degradation of polymer chains during processing could also occur. Consequently, the quality of recycled materials decreases with each recycling cycle, often reducing the performance in key properties, thus restricting the potential applications of recycled PET.[2–8]

[a]*Syensqo, Research and Innovation Center of Shanghai, Eco-Efficient Products and Processes Laboratory, 3966 Jindu Road, Xinzhuang Industrial Zone, Shanghai, China. E-mail: antoine.beuque@syensqo.com*

[b]*Syensqo, Research and Innovation Center of Lyon, 85 Avenue des Frères Perret, 69190 Saint-Fons, France*

[c]*Centre National de la Recherche Scientifique, Eco-Efficient Products and Processes Laboratory, IRL 3464, 3966 Jindu Road, Xinzhuang Industrial Zone, Shanghai, China*

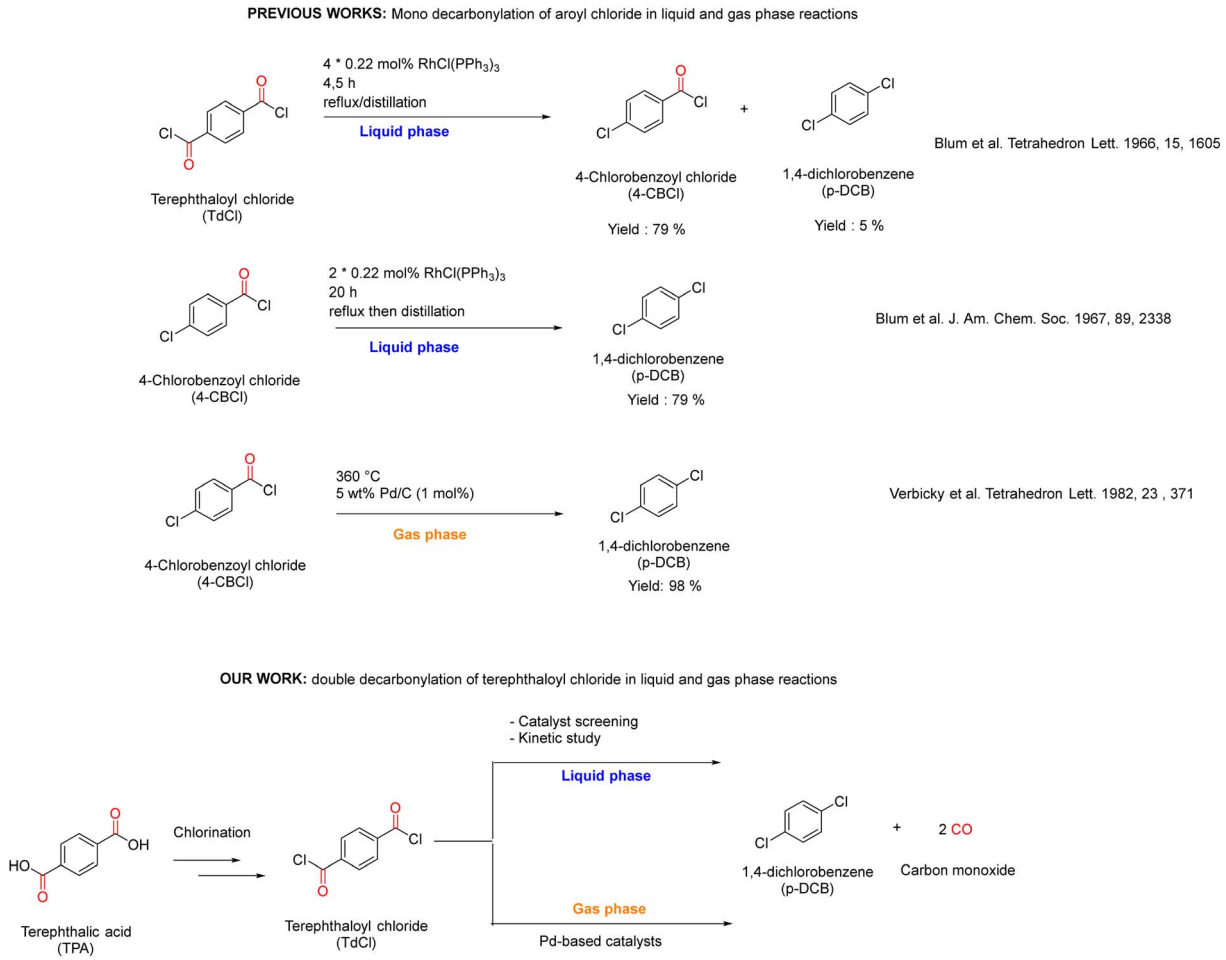

Fig. 1 Prior reports and our work on liquid and gas phase decarbonylation of aroyl chloride.

To address this limitation, the use of controlled polymer chain cleavage *via* chemical and biological post-treatments has emerged as a promising solution, leveraging the presence of labile ester bonds in PET.[9,10] By depolymerizing PET into its monomeric building blocks without causing molecular degradation, this approach enables the reuse of the polymer with minimal loss in quality.[6,11]

Various companies are developing pioneering processes to recycle post-consumer PET waste into high-purity monomers. Notable technologies include methanolysis (Loop Industries[12] and Eastman Chemical[13]), glycolysis (Ioniqa Technologies[14]), alkaline hydrolysis with UV activation (DePoly[15]), and enzyme-based recycling (Carbios[16]).

Collectively, these technologies are expected to process hundreds of millions of tons of post-consumer PET waste annually, positioning TPA as an emerging, highly functional, and valuable building block for a wide range of industrial applications.

As part of its sustainability ambition, Syensqo is committed to advancing the circular economy. This is ensured by increasing its share of circular products and solutions in the portfolio by 2030.[17] Syensqo commercializes a high-performance polymer from *para*-dichlorobenzene (*p*-DCB) for automotives and electronic applications—polyphenylene sulfide (PPS) Ryton® polymer.[18]

p-DCB is produced directly from chlorination of benzene with a strong Lewis acid ($FeCl_3$, $AlCl_3$, …).[8] This fossil-based route involves numerous toxic chemicals, produces lot of chemical wastes and requires further steps to separate the isomers and purify the final *p*-DCB.[19]

In this context, our approach focuses on developing more sustainable synthesis pathways for *p*-DCB, enabling the production PPS polymer in response to the growing demand for sustainability. Specifically, given the anticipated increased availability of recycled terephthalic acid, the conversion of TPA to *p*-DCB emerges as a particularly attractive approach.

To consider this alternative route to *p*-DCB, terephthaloyl chloride (TdCl) derived from TPA was first obtained. Subsequently, TdCl underwent two sequential decarbonylation steps to yield *p*-DCB, releasing two moles of carbon monoxide (CO). This double decarbonylation was identified as the key challenge in the overall process and therefore constituted the primary focus of our investigation. In our study, we assessed its feasibility by using two different strategies: liquid phase and gas phase reactions (Fig. 1).

The liquid phase decarbonylation of aroyl chlorides was reported in the early 1960's by Blum *et al.* using the well-known Wilkinson's catalyst, the rhodium(I) complex $RhCl(PPh_3)_3$. They reported the monodecarbonylation of TdCl to 4-chlorobenzoyl chloride (4-CBCl) with a notable yield of 79% under dry and inert conditions, along with the formation of 5% of *p*-DCB. The resulting intermediate 4-CBCl could be further converted to *p*-DCB with a 79% yield using the same catalyst in a separate, second step (Fig. 1), requiring a longer reaction time.[20–23]

Two decades later, the only example of heterogeneous decarbonylation of aroyl chloride in the gas phase was reported by Verbicky *et al.* Using a highly loaded palladium catalyst (5 wt% on carbon), the decarbonylation of 4-CBCl in the gas phase afforded an excellent 98% yield of *p*-DCB at 360 °C. It is worth mentioning that the nature of the *para*-group drastically impacts the catalytic activity with no evident correlation. As an example, the decarbonylation of the nitrobenzoyl chloride afforded only 7% of its chloro product under the same conditions (Fig. 1).[24]

The routes previously reported only showed a limited scope for aroyl chloride conversion to chlorobenzene derivatives, solely focusing on the feasibility of the reaction using chlorobenzoyl chloride derivatives as substrates. Furthermore, for the liquid-phase reactions, critical procedural details like the gradual and repeated addition of catalyst, multiple cycles of reflux heating, and distillation are intricately described. Regarding the gas phase, essential parameters like the weight hourly space velocity (WHSV) and gas feed composition are also not reported (Fig. 1). Notably, these studies addressed only the mono-decarbonylation of aroyl chlorides, leaving the double decarbonylation unexamined. This lack of clear understanding and the unexplored range of substrates prompted us to start this study.

To address these missing points, we conducted a comprehensive study on the feasibility of the double decarbonylation of terephthaloyl chloride, exploring both liquid and gas phase catalysis.

First, the liquid phase decarbonylation of TdCl was investigated in a simple one-pot reaction. Catalyst screening was conducted to identify the most active catalyst. Then, the experimental conditions of the reaction were optimized by evaluating the impact of several experimental parameters, including the catalyst amount and reaction time.

In the second part of this study, the gas-phase decarbonylation of TdCl was carried out using two Pd-based catalysts with different supports (alumina and carbon) at various contact times. A subsequent kinetic study was realized, revealing catalyst deactivation for both types of supports. Characterization of the recovered spent catalysts provided further insight into the possible *in situ* generation of the active palladium phase and the mechanisms of catalyst deactivation.

2. Experimental

2.1. Liquid phase decarbonylation of TdCl

2.1.1. Materials. All purchased reagents were used without additional purification unless otherwise indicated. Terephthaloyl dichloride (purity > 99%) and the Wilkinson catalyst, tris(triphenylphosphine)rhodium(I) chloride (purity > 99%), $RhCl(PPh_3)_3$, were purchased from Tokyo Chemical Industry Co., Ltd.

Bis[tris(2-methylphenyl)phosphine]palladium(0) (purity > 97%), $Pd[P(o\text{-tol})_3]_2$ (product number: 711071); tris(dibenzylideneacetone)dipalladium(0) (purity > 97%), Pd_2dba_3 (product number: 328774); 2-(dicyclohexylphosphino)3,6-dimethoxy-2′,4′,6′-triisopropyl-1,1′-biphenyl (purity > 98%), BrettPhos (product number: 718742); 4,5-bis(diphenylphosphino)-9,9-dimethylxanthene (purity > 97%), Xantphos (product number: 526460); and bis(1,5-cyclooctadiene)diiridium(I) dichloride (purity > 97%), $[Ir(cod)Cl]_2$ (product number: 683094); rhodium on carbon, extent of labeling: 5 wt% loading (product number: 206164), were purchased from Sigma-Aldrich Co. LLC.

Triphenylphosphine (purity > 99%), PPh_3Cl_2 (product number: L02502), was purchased from Thermo Fisher Scientific Inc.

Due to the potential air-sensitivity of the purchased chemicals, they were stored inside the glovebox under an argon gas atmosphere after their purchase.

2.1.2. Experimental setup. The liquid phase catalytic experiment was carried out in a reflux setup under a N_2 inert atmosphere. A small round bottom flask of 5 mL volume was connected to a condenser and placed in an oil bath for heating. The outlet of the condenser comprised a valve directly connected to an oil trap followed by a CO detector to monitor online the CO production and take all the precautions necessary with this toxic gas (Fig. S1). All experiments were performed neat.

2.1.3. Liquid phase catalytic reaction. The round bottom flask was loaded with 1 g of TdCl, the desired amount of catalyst (0.05–2 mol%) and the ligand (0–2 mol%) and placed inside a glovebox. A small stirrer was also added. It was sealed and transferred to the experimental setup. The liquid phase reaction was carried out under solvent-free conditions. The setup was initially purged with N_2 using a Schlenk line connected to the top of the condenser. The valve was opened. After purging the system, the N_2 flow was kept constant, and the round bottom flask was quickly connected to the setup, making sure the joints were sealed correctly and the valve was closed. Then, the outlet of the condenser was connected to the oil trap and CO-detector, and the valve was opened.

The reaction temperature was set at 220 °C, and the stirring rate was set to 1000 rpm for 7 hours. TdCl melted around 80 °C. Bubbling in the oil trap was observed around 200 °C, indicating the release of CO. When no more CO was generated, the reaction was considered complete. The setup was then cooled down to room temperature and open to air. The crude reaction mixture was dissolved in 25 mL of dichloromethane (DCM) prior to GC analysis (CS25). Then, the solution was further diluted by a factor of 50 in DCM prior to LC analysis (CD50).

2.2. Gas phase decarbonylation of TdCl

2.2.1. Materials. Prior to the reaction, 5 wt% Pd/Al_2O_3 purchased from Johnson Matthey (A302099-5) was compacted

under 3 tons of strain using a hydraulic press, crushed, and sieved to obtain particles with an homogeneous distribution of size (0.4–0.8 mm). 3.3 wt% Pd/C purchased from Johnson Matthey as small extrudates ($Ø = 1$ mm $\times$ $l = 3$ mm) was directly used.

2.2.2. Experimental setup. Due to the high melting point (83 °C) and boiling point (259 °C) of TdCl, the gas phase decarbonylation of TdCl faces initial technical challenges. To remediate this issue, an Effi Microactivity FR 200 reactor from Micromeritics was slightly modified by adding a bubbler inside the hotbox, upstream of the reactor, to melt TdCl and bubble N_2 through it to generate and transport its vapor (Fig. S2).

Preliminary calibration curves at different temperatures of the hotbox were calculated for TdCl. Upon heating the hotbox at 200 °C under a N_2 flow of 100 mL min^{-1}, the average mass flow of TdCl was 366 mg h^{-1} with a standard deviation of ~10% (Table S1).

Prior to the catalytic test, the thermal stability of the starting material (TdCl) and intermediate (4-CBCl) was assessed using differential scanning calorimetry (DSC) analysis under an inert atmosphere up to 400 °C. No exothermic peaks were observed, indicating thermally stable reagents (Fig. S3).

2.2.3. Gas phase catalytic reaction. A stainless-steel reactor column with an inner diameter of 1 cm was loaded with the required amount of catalyst (50–300 mg). A stainless-steel bubbler was also loaded with 4 g of TdCl inside the glovebox and transferred to the Effi microactivity system. A nitrogen flow of 100 mL min^{-1} at 1 atm was set to keep the catalyst and substrate under an inter atmosphere.

The hotbox was heated at 200 °C, the reactor to the desired reaction temperature (360 °C) and the external line at 250 °C. When thermal equilibrium was reached, the N_2-flow was opened and set to 100 mL min^{-1} at 1 atm. A pressure gauge was installed at the reactor inlet to monitor the pressure system online. The total weight hourly space velocity (WHSV) was between 25 h^{-1} and 150 h^{-1}.

After 1 hour of reaction, the heating of the hotbox, reactor, and external lines was stopped, and the hotbox was opened to favor the rapid quenching of the reaction (5 min to reach 30 °C) inside the boiler (below the melting point of TdCl). The collection system can be disassembled for analysis of reaction products collected in the Schlenk. The spent catalyst was also recovered for analysis.

Similar to the liquid phase reaction, the crude reaction mixture was dissolved in 25 mL of DCM prior to GC analysis (CS25). Then, the solution was further diluted by a factor of 50 in DCM prior to LC analysis (CD50).

2.3. Product identification and quantification

In this study, a dual analytic method, gas/liquid chromatography (GC/LC), was used. A GC was coupled with a flame ionization detector (FID) and a mass spectrometer (MS) detector. The dissolved crude sample in 25 mL of DCM (CS25) was analyzed using an Agilent 7890B GC equipped with an Agilent CP7727: CP-Wax 58 FFAP CB capillary column of 30 m $\times$ 0.25 mm $\times$ 0.25 μm dimensions. An optimized temperature program allowed the baseline separation of all compounds: the column temperature was stable at 40 °C during 5 min. Then, it was increased from 40 °C to 250 °C at a rate of 10 °C min^{-1}, and kept constant for 5 min.

In parallel, the diluted sample (CD50) was analyzed with an Agilent 1260 LC infinity instrument equipped with a C18 column of 5 μm $\times$ 4.6 $\times$ 250 mm dimensions. The LC was also equipped with an evaporative light scattering detector (ELSD), a mass spectrometer (MS) detector and an ultraviolet-diode array detector (UV-DAD) to quantify the high boiling point chemicals.

The mobile phase constituted a mixture of water with 0.1% volume of formic acid and acetonitrile. The gradient was kept at 100% water for 1 min. Then, acetonitrile was added progressively to reach a mixture of 70/30 (v/v) water/acetonitrile at 26 min. This concentration was maintained for 1 min. Afterward, the concentration of water was decreased to 0% in 3 min. This analytical method is performed at a constant temperature of 40 °C. The analyses were conducted simultaneously using a DAD (used for quantification) and a MS detector. The MS permitted the verification of peaks identified by retention time with the DAD and the identification of by-products.

The molar yield of the products and the conversion of TdCl were calculated using calibration curves. Calibration curves were constructed for each main component. Calibration curves for TdCl and 4-CBCl were measured on the LC-UV-DAD. Calibration curves for *p*-DCB, ClB and PCB-15 were measured on the GC-FID (Fig. S4).

The turnover number (TON) and turnover frequency (TOF) of *p*-DCB were calculated according to the following equations:

$$\mathrm{TON} = \frac{\mathrm{mol}(p\text{-DCB})}{\mathrm{mol\ of\ catalyst}} \quad (1)$$

$$\mathrm{TOF}\left(h^{-1}\right) = \frac{\mathrm{TON}}{\mathrm{reaction\ time}} \quad (2)$$

2.4. Characterization of the spent catalysts

Coke amount was quantified with a SDT Q600 at a flow rate of 100 mL min^{-1} air up to 800 °C. After loading the thermogravimetric cell, the sample was first kept for 30 min in a dry air stream at room temperature. Then, it was heated with a rate of 2 °C min^{-1}. Once the final temperature was reached, the plateau was held for 10 min.

Powder X-ray diffractograms were collected with an X'Pert^3 Malvern Panalytical X-ray diffractometer with Cu K_α radiation ($\lambda = 0.15418$ nm), within a 2θ range between 10° and 90°. The scan rate was fixed at 0.0167° s^{-1}.

Dichloromethane (DCM) extraction of the spent catalyst was performed at room temperature under stirring for 24 h in 50 mL of DCM in a closed flask. After filtration, LC analysis was performed using the methodology described previously.

X-ray fluorescence (XRF) data were recorded with a Malvern Panalytical ZETIUM XRF elemental analyzer. The data were analyzed using Omnian application, which is the standard-free method for semiquantification.

2.5. Density functional theory calculations (gas phase reaction)

Our calculations were carried out using the VASP 5.4 package within the periodic density functional theory (DFT) framework, employing the Perdew–Burke–Ernzerhof (PBE) exchange–correlation functional and a plane-wave energy cutoff of 500 eV. Gamma-centered *k*-point meshes were used, with a $5 \times 5 \times 1$ grid for slab calculations and a $30 \times 30 \times 30$ grid for bulk calculations, following the Monkhorst–Pack scheme. The electronic convergence criterion was set to 10^{-6} eV for wavefunction optimization, and the force convergence threshold for ionic relaxation was 0.05 eV. All calculations were performed at 0 K, without zero-point energy (ZPE) or entropy corrections. Pd, Al_2O_3 (gamma phase), and C (graphite phase) surfaces were constructed along the (111), (110), and (001) facet orientations, respectively, based on DFT pre-optimized bulk structures sourced from the American Crystallographic Database. Each slab model has a thickness of approximately 6–8 Å, a unit cell area between $\sim 7 \times 7$ Å^2 and $\sim 8 \times 8$ Å^2, and a vacuum spacing of at least 15 Å along the *z*-axis to prevent interaction between virtually replicated images. Only one surface type was simulated for Pd and C, and one pristine surface was considered for Al_2O_3. Additionally, for Al_2O_3 and C, all layers were allowed to relax, whereas for Pd, the two bottom layers were frozen in a bulk-like geometry. An isolated Cl atom was adsorbed onto each surface, maintaining a minimal and consistent coverage in all cases. The adsorption energy of Cl (E_{ads}(Cl)) was computed according to eqn (1), with the previously selected technical parameters ensuring convergence within 0.05 eV. Structural coordinates for all three surfaces are available in the SI.

$$E_{ads}(Cl) = E(slab\_Cl) - [E(slab) + 1/2E(Cl_2(g))], \quad (3)$$

where E(slab_Cl) is the energy of the slab with the Cl adsorbate, E(slab) is the energy of the bare slab, and $E(Cl_2(g))$ is the energy of chlorine in the gas phase.

3. Results and discussion

3.1. Liquid phase decarbonylation of terephthaloyl chloride

3.1.1. Catalyst screening. The potential active catalysts for the decarbonylation of terephthaloyl chloride in the liquid phase was selected based on active catalysts previously reported for decarbonylation reactions involving chloroaromatic derivatives (Table S2): decarbonylation of chloro-aldehyde (79% yield),[25] decarbonylative cyanation of 4-chlorobenzoyl (96% yield),[26] decarbonylative cross-coupling of *p*-nitrobenzoyl (82% yield),[27] decarbonylative nucleophilic halogenation of 4-chlorobenzoyl (85% yield),[28,29] *etc*. The selected catalysts were then evaluated for the double decarbonylation of TdCl to *p*-DCB in the liquid phase.

The catalytic performance of the selected catalysts is summarized in Table 1. Two main products were identified: the mono-decarbonylated intermediate, 4-chlorobenzoyl chloride (4-CBCl), and the di-decarbonylated product, *para*-dichlorobenzene (*p*-DCB).

As shown in Table 1, the previously reported $RhCl(PPh_3)_3$ complex (Wilkinson's catalyst, Table 1 – entry 1) was definitely the most active catalyst. It achieved 74% yield in *p*-DCB with 100% of TdCl conversion.

All the other catalysts showed no catalytic activity toward *p*-DCB, and the TdCl conversion was lower than 50% (Table 1 – entries 2–5). These catalysts (Ir, Ni, and Pd) were only active to produce a limited amount of mono-decarbonylated intermediate (4-CBCl). They appeared to lack the catalytic activity required to promote the second decarbonylation step leading to *p*-DCB.

Given that the Wilkinson catalyst demonstrated the highest activity for *p*-DCB formation, a comparative experiment was conducted using rhodium supported on charcoal (Rh/C) in the liquid phase (Table 1 – entry 6), maintaining the same molar substrate/metal ratio. In this case, the catalytic activity was markedly diminished, with only 30% conversion of TdCl, and merely trace amounts of *p*-DCB were detected. The heterogeneous Rh-based catalyst in the liquid phase produced *ca.* 9% of the intermediate (30% selectivity). Similar to the Ir-, Ni-, and Pd-based catalysts, Rh/C was insufficiently active to facilitate the second decarbonylation step.

Based on the catalyst screening results, the Wilkinson catalyst, originally reported in the 1960s for the mono-decarbonylation of 4-CBCl to *p*-DCB, also exhibited the highest catalytic activity for the double decarbonylation of TdCl to *p*-DCB. Hence, this catalyst was selected for further investigation of the double decarbonylation reaction in the liquid phase.

3.1.2. Impact of the Wilkinson catalyst amount. Fig. 2 shows the product distribution and the calculated TON as a function of catalyst loading after 7 hours of reaction. The catalyst loading was adjusted from 0.05 mol% to 2 mol%.

First, after 7 hours of reaction, the TdCl conversion exceeded 95% when the catalyst loading was higher than 0.1 mol%. In contrast, at a very low catalytic amount (0.05 mol%), the TdCl conversion decreased to 86%.

From Fig. 2, it can be seen that adding a higher catalyst amount will gradually enhance the selectivity toward *p*-DCB. At low catalyst loadings (<0.05 mol%), considerable formation of the mono-decarbonylated intermediate, 4-chlorobenzoyl chloride (4-CBCl), is observed, with its selectivity reaching 93%. In the meantime, the yield of *para*-dichlorobenzene (*p*-DCB) remains limited at 5.2%. By increasing the catalyst amount from 0.05 mol% to 0.25 mol%, a significant increase in the *p*-DCB yield, from 5.2% to 58%, is observed. This is accompanied by a decrease in 4-CBCl selectivity, from 92% to 40%. Further increasing the catalyst loading to the range of 0.5–1 mol% results in stabilization of the product distribution, with a *p*-DCB yield of approximately 90% and a 4-CBCl yield between 5% and 8%. Surprisingly, at a higher catalyst loading of 2 mol%, a slight decline in catalytic performance is observed, as evidenced by a decrease in the *p*-DCB yield to 74% and an increase in 4-CBCl selectivity.

Additionally, two minor by-products are identified: chlorobenzene (ClB) and 4,4-dichlorobiphenyl (4,4-DClBP). Regardless of the catalyst loading, the yield of 4,4-DClBP remains consistently around ~1%. A similar trend is also observed for ClB.

Table 1 Catalyst screening for the liquid phase decarbonylation of terephthaloyl chloride. Reaction conditions: 220 °C, 7 h, no solvent, 1 atm N_2 and the catalyst amount was kept constant at 2 mol%

	Catalytic system			Catalytic performance		
		Ligand			Yield (%)	
Entry	Catalyst	Name	Amount (mol%)	Conversion (%)	4-CBCl	*p*-DCB
1	$RhCl(PPh_3)_3$	—	—	100	14.5	74.2
2	$[IrCl(cod)]_2$	PPh_3	4	30	1.1	0.1
3	$Pd[P(o\text{-}tol)_3]_2$	BrettPhos	2	46	4	~0
4	$Pd_2(dba)_3$	Xantphos	4	50	20	0
5	5 wt% Rh/C	—	—	30	9.1	0.3

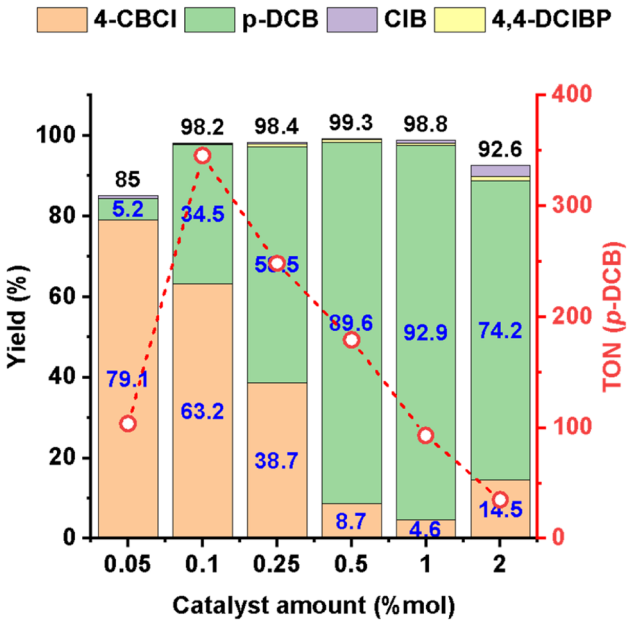

Fig. 2 Product distribution and TON obtained as a function of $RhCl(PPh_3)_3$ amount. Experimental conditions: 220 °C, 1 g of TdCl, 1 atm N_2, 7 hours, no solvent. The calculated sum of the product yield is considered as the conversion of TdCl.

However, with an excess of catalyst amount (2 mol%), an increased formation of chlorobenzene as a by-product (3% yield) is quantified.

Due to the stable *p*-DCB distribution when the catalyst loading exceeds 0.5 mol%, the *p*-DCB TON follows a bell-shaped curve reaching a maximum of 310 for 0.1 mol% (Fig. 2). However, as mentioned above, the decarbonylation of TdCl is predominantly limited to the formation of the intermediate at a low catalyst amount. In this case, the final process would require separation and recycling of the intermediate to be further converted into *p*-DCB.

These results indicate that higher catalyst loading promotes the second decarbonylation, which might be the rate-limiting step of the reaction. Several reports also indicate that the nature of the *para* group substituent on the aroyl chloride significantly impacts the catalytic performance. As an example, one can note that the reported decarbonylation of benzoyl afforded 11% higher yield than the decarbonylation of 4-CBCl under identical conditions.[21,22]

Based on these findings, a catalyst loading of 1 mol% was selected for further studies.

3.1.3. Kinetic study. To gain deeper insight into the mechanisms involved in the formation of the desired product, intermediate and by-products, a detailed kinetic study was carried out. The reaction was initiated several times under the exact same conditions and stopped at different reaction times to quantify the obtained mixture.

During the early stages of the reaction, *i.e.*, before 30 min, TdCl is converted to the mono-decarbonylated product (4-ClBC) with 100% selectivity, making this intermediate the primary product of the reaction. Once its amount reaches an optimal concentration, it undergoes further conversion into the di-decarbonylated product, *p*-DCB. The latter appears after 1 hour of reaction as the secondary product. Its selectivity significantly increases from 9% after 1 h to 94% after 4 h of reaction. After 4 hours of reaction, the reaction seems to stabilize, as the product distribution remains constant (Fig. 3). Furthermore, the calculated turnover frequency (TOF) for *p*-DCB is the highest after 2 hours of reaction, reaching 30 h^{-1}.

Regarding the formation of by-products, the yield of ClB increases progressively, reaching 1.5% yield after 7 hours. In contrast, the yield of 4,4-DClBP seems to reach a maximum value of ~1% after 4 hours of reaction. The formation of both undesirable by-products (ClB and 4,4-DClBP) starts after 2 hours of reaction, coinciding with a *p*-DCB yield of 77%. This suggests that these by-products originated from the second decarbonylation step, *i.e.*, during *p*-DCB formation, probably *via* parallel competitive mechanisms, such as C–H reductive elimination and aryl–aryl C–C coupling, respectively.

From the kinetic study, two main steps were observed. First, monodecarbonylation of TdCl formed 4-CBCl. The increase of its concentration will initiate the second decarbonylation to *p*-DCB. In more detail, the homogeneous decarbonylation of TdCl occurs through 4 key fundamental steps: oxidative addition, isomerization, CO dissociation and reductive elimination, as proposed by Blum *et al.* (Fig. S5).[22]

However, this mechanism is still under debate due to unclear by-product formation and the challenges associated with the accurate characterization of the catalyst throughout the reaction.[30–32] As proposed by Ehrenkaufer, the formation of ClB

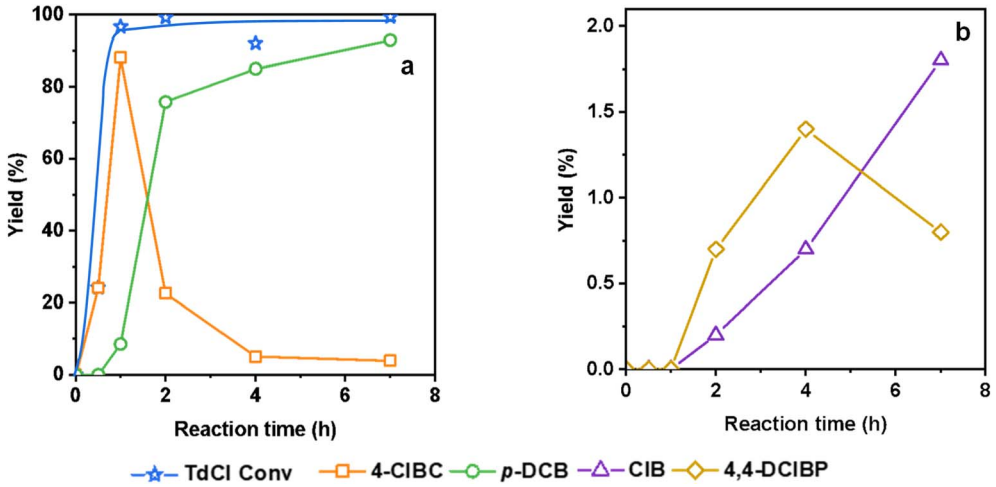

Fig. 3 Yields of 4-ClBC, *p*-DCB and TdCl conversion (a) and yields of ClB and 4,4-DClBP (b) as a function of the reaction time. Experimental conditions: 220 °C, 1 g of TdCl, 1 mol% of $RhCl(PPh_3)_3$, 1 atm N_2, no solvent.

may result from the thermal degradation of the catalytic complex at elevated temperature required for liquid phase decarbonylation.[32] Another suggestion involves the direct hydrogen transfer from the ligand to the substrate. ClB can be produced from side reactions between the ligand and the organocatalytic complex, adding further complexity to the mechanistic interpretation.

It should be noted that the 4,4-DClBP by-product is part of the polychlorinated biphenyl (PCBs) family and is also denoted as PCB-15. This group of chemicals has been banned by the Stockholm convention in 2001 due to their adverse effects on the immune system and persistence. The identification and detection of this compound and the impossibility to totally avoid its formation prompted the termination of research on this route, as it constitutes an intractable technological bottleneck to scaling up the reaction.

3.2. Gas phase decarbonylation of terephthaloyl chloride

Despite its high catalytic performance, the homogeneous decarbonylation of TdCl suffers major challenges, including the formation of traces of PCB-15 and issues related to catalyst recyclability.[33] To overcome these technological bottlenecks, the gas phase decarbonylation of TdCl was investigated. To the best of our knowledge, the double decarbonylation of TdCl in the gas phase with heterogeneous catalysts has not been previously reported in the literature, including in the reference work by Verbicky *et al.*[24]

Prior to carrying out the catalytic tests, the thermal stability of both the starting raw material and intermediate was assessed by differential scanning calorimetry (DSC) under an inert atmosphere up to 400 °C (Fig. S3). Additionally, to this thermal analysis, blank experiments at 360 °C indicated no formation of any products (Table S1). These results demonstrate that TdCl remains thermally stable up to 400 °C under an inert atmosphere.

3.2.1. Catalyst screening: influence of the catalyst support.

Two heterogeneous Pd-based catalysts were evaluated: 5 wt% Pd/Al_2O_3 and 3.3 wt% Pd/C. Fig. 4 represents the product distribution and *p*-DCB turnover number (TON) obtained with both catalysts at various weight hourly space velocity (WHSV) values, *i.e.*, the catalyst amount is adjusted.

With 5 wt% Pd/Al_2O_3, the TdCl conversion reached only ~30% for WHSV above 75 h^{-1}. At a lower WHSV (25 h^{-1}), *i.e.*, higher catalyst loading, the conversion of TdCl increased to 68%. The monodecarbonylated product formed with high selectivity (>96%), regardless of the WHSV. The remaining fraction consisted exclusively of *p*-DCB, with a selectivity lower than 4%. The TON (*p*-DCB) remained constant at ~0.2, regardless of the WHSV. The findings indicate that the Pd/Al_2O_3 catalyst was active to complete the mono-decarbonylation of TdCl to 4-CBCl, while the subsequent second decarbonylation step was significantly limited.

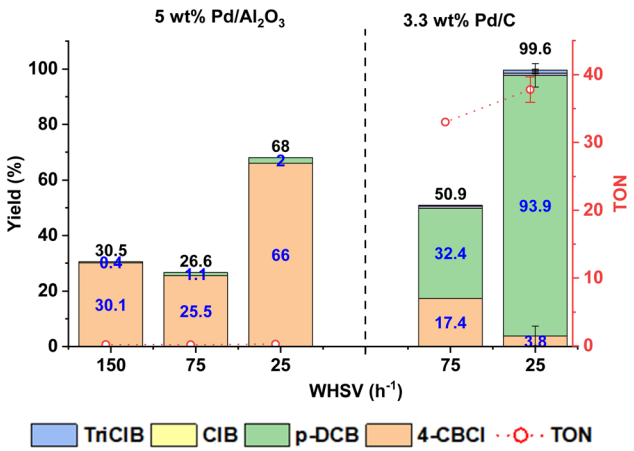

Fig. 4 Product distribution and TON (*p*-DCB) obtained with Pd/C and Pd/Al_2O_3. Experimental conditions: 360 °C, 366 mg h^{-1} TdCl, 100 mL min^{-1} N_2, 1 hour, WHSV (25–150 h^{-1}). The calculated sum of the product yield is considered as the conversion of TdCl.

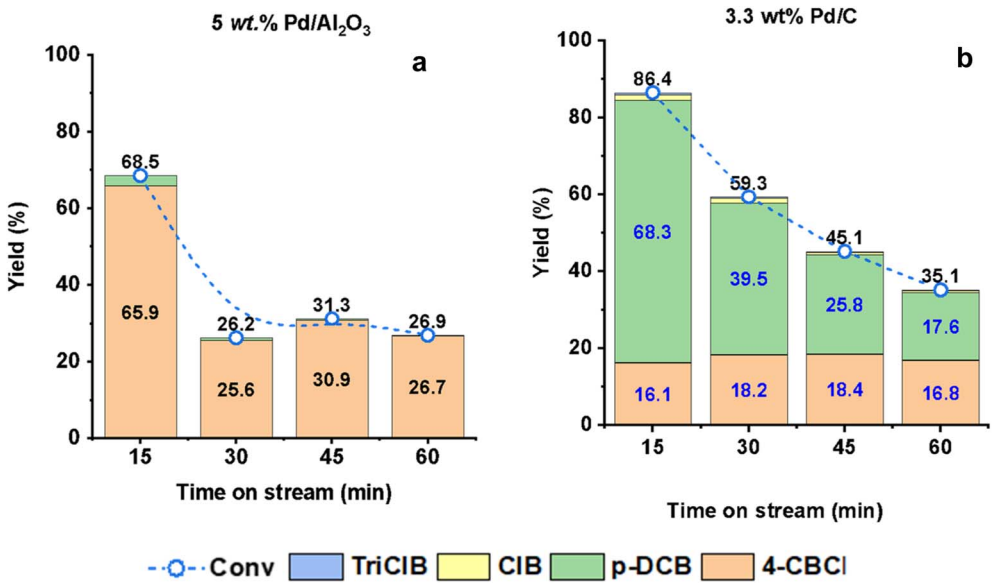

Fig. 5 Product distribution as a function of time on stream for (a) 5 wt% Pd/Al_2O_3 and (b) 3.3 wt% Pd/C. Experimental conditions: 360 °C, 366 mg h^{-1} TdCl, 100 mL min^{-1} N_2, WHSV (75 h^{-1}). The calculated sum of the product yield is considered as the conversion of TdCl.

Remarkably, changing to a carbon support drastically shifted the reaction towards *p*-DCB formation. At a WHSV of 75 h^{-1}, the TdCl conversion improved compared to the alumina support catalyst, exceeding 50%. *p*-DCB became the main product with a selectivity of 64%. By increasing the catalyst amount, *i.e.*, lowering the WHSV, complete TdCl conversion was achieved with a high yield in *p*-DCB (94%) in 1 hour at 360 °C. The TON (*p*-DCB) slightly increased from 32 to 40 as the WHSV was reduced from 75 h^{-1} to 25 h^{-1}, representing a 200 times enhancement compared to the TON (*p*-DCB) achieved with the alumina support (Fig. 4).

Additionally, it should also be noted that small amounts of by-products were also detected with the Pd/C catalyst: chlorobenzene (~1%) and trichlorobenzene (TriCl: ~0.5%). The latter was formed by *trans*-chlorination of *p*-DCB at high temperatures.[34]

The best catalytic performance at a WHSV of 25 h^{-1} was reproduced four times to assess repeatability.

These results underline the critical influence of the catalyst support on the gas-phase decarbonylation of TdCl to *p*-DCB. While the alumina support primarily afforded the mono-decarbonylated intermediate (4-CBCl) as the main product, the carbon support considerably enhanced the catalytic performance, favoring the second decarbonylation step to produce *p*-DCB. The highest calculated TON (*p*-DCB) was 40 over 3.3 wt% Pd/C, corresponding to a TOF of 30 h^{-1}, similar to the values calculated during the liquid-phase decarbonylation.

3.2.2. Kinetic study. To further investigate the observed gap in catalytic behavior, a kinetic study was conducted using both catalysts. The reaction was carried out for 1 hour. Samples were collected at 15 minute intervals and consequently analyzed to gain deeper insight into the mechanism involved in the reaction.

Fig. 5 shows the product distribution as a function of the time of stream for the two catalysts. For Pd/Al_2O_3, the initial activity (at 15 minutes) decreased by half over the following 15 minutes, dropping from ~69% to ~30%. After 30 min, the TdCl conversion remained constant. The selectivity for *p*-DCB decreased from 4% at 15 minutes to 1% at 30 minutes. Only trace amounts were detected after 30 minutes (Fig. 5a). The rest of the fraction constituted exclusively of 4-ClBC.

Similar trends were noticed with the Pd/C catalyst. The initial activity at 15 minutes had been reduced by 30% in the next 15 minutes, from ~86% to ~59%. Then, the TdCl conversion continued to decline gradually, reaching 35% after 60 minutes of reaction. The *p*-DCB selectivity also decreased from 79% to 50%, while the selectivity for the intermediate increased correspondingly (Fig. 5b). For both samples, the loss of catalytic activity and *p*-DCB productivity revealed catalyst deactivation.

According to the approach developed by Froment,[35] the loss of catalytic activity is related to different parameters (time on stream, coke content, *etc.*) following semi-empirical laws. The deactivation function, $\phi_k = \frac{r_A}{r_A^0}$ is defined as the ratio between reaction rates of the coked and fresh catalysts (eqn (4)) and its time evolution (eqn (5)). This equation contains a deactivation parameter α_t (min^{-1}).[36] Such a model does not consider the experimental conditions.

$$\phi_k = \frac{r_A}{r_A^0} \quad (4)$$

where ϕ_k: deactivation function, r_A: reaction on the coked catalyst, and r_A^0: reaction on the fresh catalyst.

$$\phi_k(t) = \exp(-\alpha_t \times t) \quad (5)$$

where α_t: deactivation constant.

This model was applied on the two Pd-based catalysts. The fitted deactivation constants are α_t (Pd/Al_2O_3) = 0.064 min^{-1} and α_t (Pd/C) = 0.033 min^{-1}. This suggests that the deactivation rate was two times faster on alumina compared to the carbon support. Additionally, with regard to the low production of *p*-DCB, the alumina support promotes the loss of catalytic activity.

3.3. Characterization of spent catalysts

To better understand the significant differences in catalytic activity and the deactivation mechanisms occurring during the gas-phase decarbonylation of TdCl, both spent catalysts were recovered at 1 hour after quenching the reaction and further characterized.

First, XRD measurements were performed to evaluate any structural change of the catalysts during the reaction. Fig. 6 presents the XRD patterns for both catalysts, before and after 1 hour of reaction. For the fresh and spent 5 wt% Pd/Al_2O_3, similar patterns are observed with diffraction peaks at $2\theta \sim$ 31.5°, 37.5°, 46.5°, 60.4°, 67.5°, and 85° and attributed to (220), (311), (400), (511), (440), and (300) planes of the γ-Al_2O_3 phase (JCPDS card no. 00-029-0063), respectively.[37] This indicates that alumina preserves its crystalline structure. Hence, no irreversible amorphization of the catalyst support occurs during the reaction.

Additionally, a small peak at $2\theta \sim 40.0°$, characteristic of Pd (111), appears on the fresh catalyst. This suggests the palladium is not initially well dispersed. After the reaction, the intensity of this peak markedly increases. Furthermore, a peak at $2\theta \sim 80.0°$ corresponding to Pd (311) emerges during the reaction.[38] The emergence and intensification of these two peaks are characteristic of the formation of larger Pd particles on the spent catalyst, confirming Pd sintering on the alumina support during the reaction (Fig. 6a).

A similar deactivation behavior was observed during the decarbonylation of heptanoic acid over Pd/C. Davis *et al.* demonstrated that at 300 °C, metal sintering occurs in the liquid phase reaction and in the gas phase reaction. Studies showed that increasing the reactant concentration promote the Pd sintering.[39]

Additional peaks at $2\theta \sim 18.9°$, 20.3°, 28.0°, 40.5°, and 53.0° were also detected. They are characteristic of the presence of aluminum hydroxide.[40] For the spent 5 wt% Pd/Al_2O_3 catalyst, the peaks associated with aluminum hydroxide disappeared.

Notable differences were observed when the catalyst support was changed. For the fresh Pd/C catalyst, the two broad peaks centered around $2\theta = 22°$ and $2\theta = 44°$ are characteristic of the amorphous carbon support. The peaks identified at 40.1°, 46.6°, 68.1° and 82.4° correspond to the (111), (200), (220) and (311) crystal plane diffraction peaks of the face-centered cubic structure of Pd (JCPDS card, file no. 46-1043), respectively.[38]

After 1 hour of reaction, a slight shift of the characteristic palladium peaks to lower 2θ values was observed, suggesting an increase in the interplanar spacing of the crystal lattice. This shift may be attributed to a phase transformation by crystal structure change or from lattice expansion caused by the insertion of larger atoms into the Pd particles.[41,42] Previous studies have reported that a palladium carbide phase (PdC_x) formed when palladium was exposed to an atmosphere of carbon monoxide and heated at temperatures higher than 350 °C.[43]

During the decarbonylation of TdCl over the Pd/C catalyst, CO was released and underwent non-dissociative adsorption on the palladium surface. Consequently, the elevated reaction temperatures promoted the rapid CO dissociation over Pd, leading to the incorporation of atomic carbon into the bulk palladium phase which shifted the Bragg reflection to smaller 2θ values.[44] The *in situ* formation of the palladium carbide phase was shown to promote both the adsorption and the production of CO.[45] This change of palladium phase was not observed on the alumina support and might be the cause of the lower catalytic activity on this support.

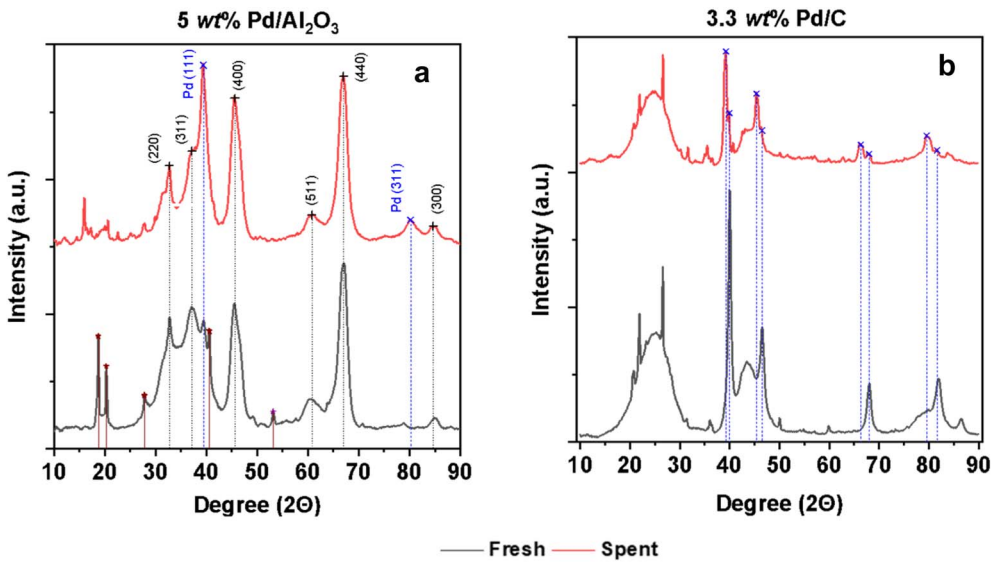

Fig. 6 XRD patterns of the fresh and spent catalysts recovered after 1 hour of reaction for (a) 5 wt% Pd/Al_2O_3 and (b) 3.3 wt% Pd/C.

Table 2 Amount of the total coke recovered on the spent catalyst and nature and amount of coke recovered during DCM extraction; N.D.: not detected

	Coke on the spent catalyst after the reaction			DCM extraction	
Catalyst name	Mass before the reaction (mg)	Mass after the reaction (mg)	Total coke (wt%)	4-CBCl (wt%)	*p*-DCB (wt%)
5 wt% Pd/Al_2O_3	300	345	12.6[a]	0.4	N.D.
3.3 wt% Pd/C	300	327	8.2[b]	N.D.	1.1

[a] Measured by TGA. [b] Measured with a precision balance.

Further thermogravimetric analyses (TGA) were performed to quantify the carbonaceous deposit, known as coke, on the 5 wt% Pd/Al_2O_3 catalyst. However, due to the characteristics of the carbon support, TGA was not applicable to the Pd/C catalyst. Instead, the amount of carbonaceous deposit on this catalyst was determined by directly measuring its total mass after removal from the reactor using a precision balance.

From Table 2, based on direct measurement with a precision balance, 8.2 wt% of coke was quantified on the carbon support. On the alumina support, 12.6 wt% of coke was measured with TGA analysis. As a matter of fact, the acid site generated by the hydroxyl group of the alumina could lead to an acid-catalyzed site reaction, generating coke by the polymerization reaction. Thus, the hydroxyl groups are presumably recovered by accumulated carbonaceous species side products that are strongly adsorbed.[39]

The accumulation of carbon deposit on both catalysts could be the cause of the observed catalyst deactivation by blocking the access of the active sites.

To further investigate the chemical structure of the carbonaceous deposit, the spent catalysts were extracted with dichloromethane (DCM) at room temperature by simple stirring. After extraction, the solutions were analysed by liquid chromatography. Table 2 presents the nature and the quantity of the coke extracted.

For the Pd/Al_2O_3 catalyst, the DCM extraction revealed the small presence of 4-chlorobenzoyl (4-CBCl). No *p*-DCB was detected after the DCM extraction. This suggests that the intermediate is strongly adsorbed on the catalyst. The recovered amount of 4-CBCl represents only 3% of the total coke, indicating that the majority of the deposited coke is of different nature. Several studies have shown that chlorinated compounds could also lead to catalyst deactivation of Pd/Al_2O_3. During the hydrodechlorination of chlorobenzene over Pd/Al_2O_3, deactivation of the metal center has been attributed to poisoning by the generated HCl, although chlorobenzene (ClB) itself was not detected as being adsorbed on the Pd particles.[46] Other research studies also indicate that ClB and benzoyl chloride could also be adsorbed on γ-Al_2O_3.[47,48]

In parallel, the weight loss identified by TGA reasonably corresponds to heavy coke deposition that is impossible to extract easily with DCM at room temperature, possibly due to interaction with alumina hydroxide species.[39]

From the XRD analysis and TGA, two deactivation mechanisms were suggested for the Pd/Al_2O_3 catalyst: (i) palladium sintering and (ii) heavy carbon deposition on the alumina support. Typically, when chloroaromatic compounds were used as starting materials, a similar deactivation pattern was also noticed for Pd/Al_2O_3.[49]

Regarding the Pd/C catalyst, no 4-CBCl was detected after DCM extraction. Only 1.1 wt% of *p*-DCB was identified, accounting for over 13% of the total weighed coke. Similar to the Pd/Al_2O_3 catalyst, this indicates the presence of additional carbonaceous species on the spent catalyst that are not extractable under these conditions.

To gain further insight into the species deposited, particularly on the active Pd/C catalyst, the fresh and spent 3.3 wt% Pd/C catalysts were analyzed using the X-ray fluorescence (XRF) semi-quantitative methodology (Table S3). On the fresh catalyst, only a small amount of Cl was noticed ($\sim$0.2 wt%). After 1 hour of reaction, the relative amount of Cl deposited on the catalyst drastically increased, exceeding 10 wt%. On the spent catalyst, the molar ratio Cl/Pd increased up to 8.5. After DCM extraction, this molar ratio decreased to $\sim$6. This indicates that approximately 30% of the total adsorbed chlorinated compounds were removed by extraction. These findings suggest that, in addition to the extracted *p*-DCB, a significant amount of chlorinated species remained strongly adsorbed on the catalyst.

3.4. Modelling

As we observed in our experimental tests, the catalyst support is essential for its activity and selectivity. Although its precise function in the chemical process is still not fully understood, DFT computations can help clarify its role and offer valuable insights into the reaction mechanism during the initial stages of the reaction. Given the significant impact of the support, it is likely that the active site is located near the metal–support interface, with both the metal and the support acting synergistically. We propose the following mechanism: (1) initially, a concerted step leads to the simultaneous cleavage in TdCl of the C–C bond between the aromatic ring and the carbonyl group, as well as the C–Cl bond between CO and Cl. This results in the release of a CO gas molecule, while an aryl radical and a Cl adatom are formed (see Fig. 7a). (2) Finally, the aryl radical and the Cl adatom combine to produce 4-CBCl. This process is then repeated with 4-CBCl to obtain *p*-DCB. While the aryl radical generated in step (1) is likely to remain strongly

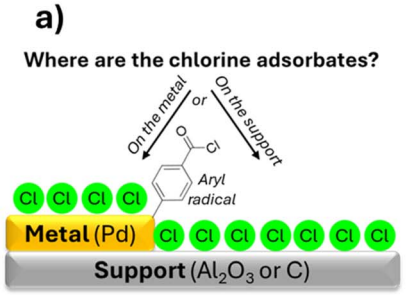

b)

Surface	E_{ads}(Cl)
Pd (metal)	0.03 eV
C (graphite)	2.58 eV
Al_2O_3 (pristine)	0.92 eV

Fig. 7 Schematic representation of the aryl radical intermediate at the metal/support interface with Cl coverage (a); DFT-computed adsorption energies of Cl adsorbates on various types of surfaces (b).

anchored to the edge of the metal particle, the Cl adatom may undergo spillover depending on its affinity for the support.

According to our DFT calculations (see Fig. 7b), Cl is highly unstable on graphite (E_{ads}(Cl) = +2.58 eV, strongly endothermic), less unstable on alumina (E_{ads}(Cl) = +0.92 eV, moderately endothermic), and essentially thermoneutral on Pd (E_{ads}(Cl) = +0.03 eV, athermic). While these results suggest that Cl preferentially deposits on metallic sites rather than on the support, the Cl coverage on Pd is expected to be much higher in Pd/C than in Pd/Al_2O_3, since Cl adsorption is considerably more unfavorable on graphite than on alumina. Therefore, the final chlorination step involved in TdCl transformation is facilitated on Pd/C compared to Pd/Al_2O_3, as a denser Cl coverage is present in the vicinity of the aryl radical intermediate, which is adsorbed onto Pd. Recent DFT modelling also confirms that Al-doped nanotubes greatly enhance the adsorption energies of the ClB molecule caused by the electron donation from the Cl atom to the Al atom to form an Al–Cl single dative bond.[50]

Altogether, these computational results account for both the superior catalytic activity of Pd/C over Pd/Al_2O_3 and the faster deactivation experimentally observed for Pd/Al_2O_3.

3.5. Preliminary techno-economic assessment (TEA) and life cycle assessment (LCA)

As part of the work, a techno-economic assessment (TEA) and a preliminary Life Cycle Assessment (pre-LCA) of the process under study were conducted from the block flow diagram presented in Fig. S7 (the detailed methodology is provided in SI, part S.4). Briefly, the process consists of three main sections: (i) chlorination of TPA, (ii) decarbonylation of TdCl, and (iii) purification of the resulting mixture to obtain *p*-DCB. Due to the higher carbon footprint and price of rhodium (approximately 10 times higher than palladium)[51] and the regulatory constraints on the by-products generated in the liquid-phase route, the FMC assessment was performed for the gas-phase decarbonylation.

Beyond the overall FMC (Full Manufacturing Cost), the methodology provides a detailed breakdown of costs and environmental footprint by category (*e.g.*, raw materials, energy, waste treatment, or process complexity through depreciation). Given the large production scale considered (10 kt per year), both depreciation and fixed operating costs remain within a reasonable range. The analysis therefore focuses primarily on variable costs and the associated carbon footprint.

Under optimization of the gas phase decarbonylation, the cost of producing *p*-DCB *via* the heterogeneous gas phase reaction is about 5 times higher than the market price of *p*-DCB. Regarding the global warming potential (GWP) ratio, it is also about 3.5 times higher.

By category decomposition, raw materials represent a substantial share of the overall operating costs, with particularly significant contributions from thionyl chloride and palladium. By contrast, nitrogen (used as a carrier gas for terephthaloyl chloride) has a limited cost impact when an effective recycle loop is implemented. Utilities are generally inexpensive, although their contribution to the overall carbon footprint can remain non-negligible. Off-gas treatment, largely driven by caustic scrubbing requirements (NaOH) needed for the first chlorination step, is identified as a major cost contributor, whereas waste management costs are comparatively low once streams are neutralized.

The comparative preliminary LCA study (Fig. 8) highlights that switching to a recycled feedstock (*p*-DCB ex-rTPA) does not automatically translate into an overall more sustainable route. This pattern suggests that the additional processing steps, reagents, and emission control required to convert recycled TPA into *p*-DCB can shift impacts rather than eliminate them, making the net environmental advantage uncertain.

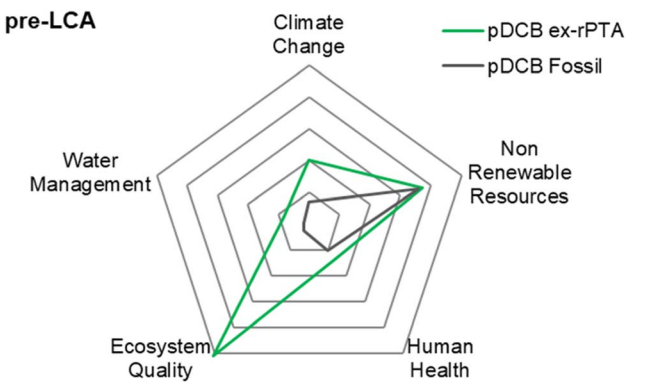

Fig. 8 Results for the whole LCA, gathered by 5 widely used categories (the smaller the surface, the lesser the impact).

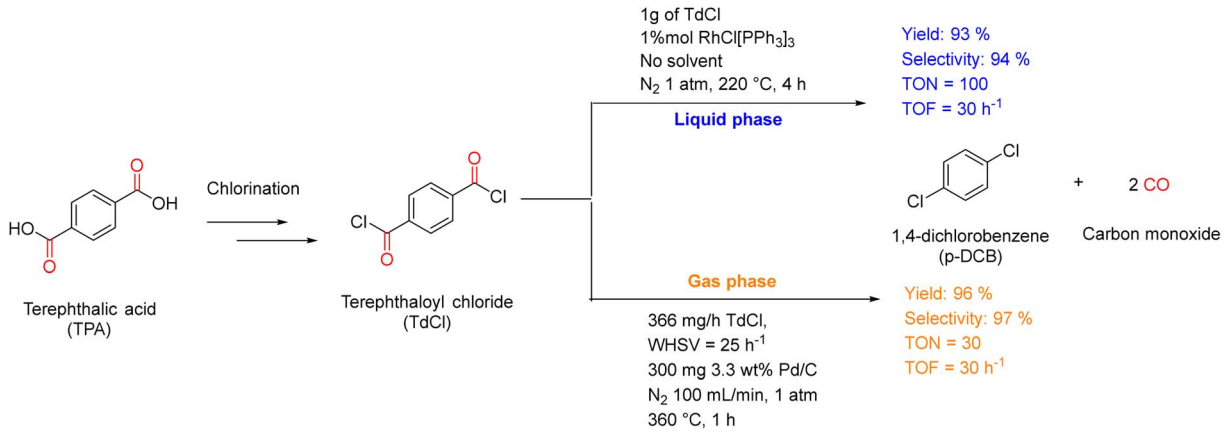

Fig. 9 Decarbonylation of terephthaloyl chloride into *p*-dichlorobenzene in liquid and gas phases.

Consequently, despite the attractiveness of circular feedstocks, this route appears challenging as a primary lever for improved sustainability unless major hotspots (*e.g.*, chlorination-related inputs and off-gas treatment) are substantially mitigated and confirmed through a full, ISO-consistent LCA with robust system boundaries and allocation choices.

When the decarbonylation section is optimized, the subsequent chlorination step becomes the predominant driver of both operating cost and environmental impact, mainly due to the consumption of thionyl chloride and the need for off-gas treatment (in addition to the baseline contribution from raw materials).

4. Conclusion

In this study, we highlight that *p*-dichlorobenzene, a key monomer in the synthesis of Ryton® polyphenylene sulfide (PPS), can be produced alternatively from terephthaloyl chloride (TdCl) derived from TPA. Notably, this work provides evidence that aroyl chlorides can undergo direct double decarbonylation to yield dichlorinated aromatic compounds in both liquid and gas phases *via* a "one-pot" process.

First, the liquid phase decarbonylation of TdCl was validated using the Wilkinson's catalyst $RhCl(PPh_3)_3$. This catalyst allowed the conversion of TdCl into *p*-DCB, achieving a maximum yield of 93% under inert and dry conditions, in neat, after 4 hours at 220 °C. The best obtained TON and a TOF in *p*-DCB were ~200 and ~30 h^{-1}, respectively (Fig. 9). However, this route suffers from the formation of trace amounts of 4,4-dichlorobiphenyl, a highly regulated by-product from the family of polychlorinated biphenyls (PCBs).

To remediate this issue, the gas phase decarbonylation of TdCl was investigated using Pd-based catalysts. Two catalysts were tested on different supports: alumina and carbon. With 5 wt% Pd/Al_2O_3, the reaction mainly produced the intermediate (4-ClBC) with high selectivity (97%) and quickly deactivated due to palladium sintering and heavy coke deposition.

By switching the catalyst support to carbon, a significant improvement in the catalytic performance was achieved. More than 95% yield of *p*-DCB was obtained in 1 hour at 360 °C with a WHSV of 25 h^{-1}. Under these conditions, TON–TOF = ~30 h^{-1}, similar to the liquid-phase pathway (Fig. 9). However, the carbon-based catalyst also suffers from loss of catalyst activity. A substantial amount of *p*-DCB and chlorinated compounds were found adsorbed on the spent catalyst. Additionally, a significant structural transformation of the Pd particles was observed, which may be associated with the formation of a reduced active phase, PdC_x.

Finally, a full manufacturing cost study of the overall process from TPA to *p*-DCB highlights that variable costs and GWP are largely driven by raw materials and off-gas treatment (Fig. 8). Future work should prioritize reducing thionyl chloride consumption (chlorination step), limiting palladium-related burdens (regeneration step development), and minimizing the cost and footprint of caustic scrubbing (NaOH) through improved gas management and recycling strategies. Nevertheless, a substantial gap remains *versus* the current fossil-based route to *p*-DCB, largely because petrochemical production benefits from highly integrated value chains (optimized energy integration, extensive co-product valorization, and strongly intensified, mature processes) and from comparatively low-cost, readily available feedstocks.

Conflicts of interest

There are no conflicts to declare.

Data availability

Data for this article, including the catalytic performance assessment, were generated during the study and are available for download as an OriginLab project file.

For the full manufacturing cost analysis and the modeling investigation, the data supporting this article are included in the supplementary information (SI). Supplementary information is available. See DOI: https://doi.org/10.1039/d5su00888c.

The exact cost and carbon footprint of the production route investigated for *p*-dichlorobenzene remain confidential.

Therefore, only a single parameter of improvement or decrease, called the *X*% factor, can be disclosed to support this study.

Acknowledgements

The authors acknowledge the support of the analytical department of the Syensqo Research Innovation Center of Shanghai for characterization of the heterogeneous catalyst. In particular, the authors would like to thank Jin Sha for the XRD, Jing Zhang for the XRF quantification, and Haobo Wang for the DSC thermal analysis.

References

1 P. Sarda, J. C. Hanan, J. G. Lawrence and M. Allahkarami, *J. Polym. Sci.*, 2022, **60**(1), 7–31.
2 T. Muringayil Joseph, S. Azat, Z. Ahmadi, O. Moini Jazani, A. Esmaeili, E. Kianfar, J. Haponiuk and S. Thomas, *Case Stud. Chem. Environ. Eng.*, 2024, **9**, 100673.
3 L. Umdagas, R. Orozco, K. Heeley and B. Al-Duri, *J. Environ. Chem. Eng.*, 2025, 119272.
4 S. S. Ali, T. Elsamahy, R. Al-Tohamy, D. Zhu, Y. A. G. Mahmoud, E. Koutra, M. A. Metwally, M. Kornaros and J. Sun, *Sci. Total Environ.*, 2021, **780**, 146590.
5 Y.-H. V. Soong, M. J. Sobkowicz and D. Xie, *Bioengineering*, 2022, **9**(3), 98.
6 C. Bharadwaj, R. Purbey, D. Bora, P. Chetia, R. U. Maheswari, R. Duarah, K. Dutta, E. R. Sadiku, K. Varaprasad and J. Jayaramudu, *Mater. Today Sustain.*, 2024, **27**, 100936.
7 E. J. P. Martin, D. S. B. L. Oliveira, L. S. B. L. Oliveira and B. S. Bezerra, *Waste Manag.*, 2021, **119**, 226.
8 E. Pinter, F. Welle, E. Mayrhofer, A. Pechhacker, L. Motloch, V. Lahme, A. Grant and M. Tacker, Circularity Study on PET Bottle-To-Bottle Recycling, *Sustainability*, 2021, **13**, 7370.
9 J. L. García, *Microb. Biotechnol.*, 2022, **15**(11), 2699.
10 H. K. Webb, J. Arnott, R. J. Crawford and E. P. Ivanova, Plastic Degradation and Its Environmental Implications with Special Reference to Poly(ethylene terephthalate), *Polymers*, 2013, 1–18.
11 I. Vollmer, M. J. F. Jenks, M. C. P. Roelands, R. J. White, T. van Harmelen, P. de Wild, G. P. van der Laan, F. Meirer, J. T. F. Keurentjes and B. M. Weckhuysen, *Angew. Chem., Int. Ed.*, 2020, **59**(36), 15402.
12 H. Essaddam, Polyethylene terephthalate depolymerization, *US Pat.,* US9550713B1, 2015.
13 A. Tullo, *C&EN Global Enterprise*, 2021, **99**(5), 10.
14 M. Gravendeel, M. de Groot, L. Slenders, B. Stevens, M. Stolk, J. Wolters, A. Wolters and F. Wouters, in *Industrial Arene Chemistry*, 2023, pp. 2117–2141.
15 M. Peplow, *C&EN Global Enterprise*, 2023, **101**(37), 22–23.
16 R. Grace, Carbios Gets Green Light to Build a PET Bio-Recycling Plant in France, *Plast. Eng.*, 2023, 1–2.
17 https://www.syensqo.com/en/our-impact/sustainability, accessed 28 September 2025.
18 *Ryton-PPS*, https://www.syensqo.com/en/brands/ryton-pps, accessed 28 September 2025.
19 G. W. Ware, in *Reviews of Environmental Contamination and Toxicology: Continuation of Residue Reviews*, ed. G. W. Ware, Springer New York, New York, NY, 1988, pp. 51–68.
20 J. Tsuji, K. Ohno and T. Kajimoto, *Tetrahedron Lett.*, 1965, **6**(50), 4565–4568.
21 J. Blum, *Tetrahedron Lett.*, 1966, (15), 1605.
22 J. Blum, E. Oppenheimer and E. D. Bergmann, *J. Am. Chem. Soc.*, 1967, **89**(10), 2338–2341.
23 J. Tsuji, K. Ono and T. Kajimoto, *Tetrahedron Lett.*, 1965, (50), 4565.
24 J. W. Verbicky Jr, B. A. Dellacoletta and L. Williams, *Tetrahedron Lett.*, 1982, **23**(4), 371.
25 T. Iwai, T. Fujihara and Y. Tsuji, *Chem. Commun.*, 2008, (46), 6215–6217.
26 Z. Wang, X. Wang, Y. Ura and Y. Nishihara, *Org. Lett.*, 2019, **21**(17), 6779–6784.
27 C. A. Malapit, N. Ichiishi and M. S. Sanford, *Org. Lett.*, 2017, **19**(15), 4142–4145.
28 Y. H. Lee and B. Morandi, *Nat. Chem.*, 2018, **10**(10), 1016–1022.
29 T. Tian, M. Kashihara, W. Yan and Y. Nishihara, *ACS Catal.*, 2024, 11905–11917.
30 J. K. Stille and M. T. Regan, *J. Am. Chem. Soc.*, 1974, **96**(5), 1508–1514.
31 J. A. Kampmeier, R. M. Rodehorst and J. B. Philip Jr, *J. Am. Chem. Soc.*, 1981, **103**(7), 1847–1849.
32 R. E. Ehrenkaufer, *ACS Catal.*, 1982, **47**, 2489–2491.
33 H. Zhao, A. K. Ravn, M. C. Haibach, K. M. Engle and C. C. C. Johansson Seechurn, *ACS Catal.*, 2024, 9708–9733.
34 K. Shinoda, *Chem. Lett.*, 1987, **16**(10), 2051–2052.
35 G. B. Marin and G. F. Froment, *Chem. Eng. Sci.*, 1982, **37**(5), 759–773.
36 O. Levenspiel, *J. Catal.*, 1972, **25**(2), 265–272.
37 A. F. Alamouti, M. Nadafan, Z. Dehghani, M. H. M. Ara and A. V. Noghreiyan, *J. Asian Ceram. Soc.*, 2021, **9**(1), 366–373.
38 B. Qi, L. Di, W. Xu and X. Zhang, *J. Mater. Chem. A*, 2014, **2**(30), 11885–11890.
39 J. A. Lopez-Ruiz, H. N. Pham, A. K. Datye and R. J. Davis, *Appl. Catal., A*, 2015, **504**, 295–307.
40 T. M. El-Sokkary, K. A. Khalil and I. A. Ahmed, *HBRC J.*, 2012, **8**(2), 91–98.
41 A. Pandey, S. Dalal, S. Dutta and A. Dixit, *J. Mater. Sci.: Mater. Electron.*, 2021, **32**(2), 1341–1368.
42 W. Vogel, W. He, Q.-H. Huang, Z. Zou, X.-G. Zhang and H. Yang, *Int. J. Hydrogen Energy*, 2010, **35**(16), 8609–8620.
43 T. Xie, Design of selective palladium-based catalyst for direct synthesis of hydrogen peroxide, PhD dissertation, The Pennsylvania State University, 2022.
44 S. B. Ziemecki, G. A. Jones, D. G. Swartzfager, R. L. Harlow and J. Faber Jr, *J. Am. Chem. Soc.*, 1985, **107**(15), 4547–4548.
45 M. A. Newton, M. Di Michiel, A. Kubacka and M. Fernández-García, *J. Am. Chem. Soc.*, 2010, **132**(13), 4540–4541.
46 N. S. Babu, N. Lingaiah, R. Gopinath, P. S. Sankar Reddy and P. S. Sai Prasad, *J. Phys. Chem. C*, 2007, **111**(17), 6447–6453.
47 L. D. Asnin, A. A. Fedorov and Y. S. Chekryshkin, *Russ. Chem. Bull.*, 2001, **50**(1), 68–72.

48 N. C. Pradhan and M. M. Sharma, *Ind. Eng. Chem. Res.*, 1992, **31**(7), 1610–1614.
49 E. López, S. Ordóñez and F. V. Díez, *Appl. Catal., B*, 2006, **62**(1), 57–65.
50 C.-H. Yeh, W.-Y. Lin and J.-C. Jiang, *Appl. Surf. Sci.*, 2020, **514**, 145897.
51 H. Zhao, A. K. Ravn, M. C. Haibach, K. M. Engle and C. C. C. Johansson Seechurn, *ACS Catal.*, 2024, 9708–9733.